The Report committee for Talha Ahmed Khan certifies that
this is the approved version of the following report:

A Stochastic Geometry Analysis of Cooperative Wireless Networks Powered by Energy Harvesting

APPROVED BY

SUPERVISING COMMITTEE:

Robert W. Heath, Jr., Supervisor

Philip V. Orlik

A Stochastic Geometry Analysis of Cooperative Wireless Networks Powered by Energy Harvesting

by

Talha Ahmed Khan, B.S.E.

REPORT

Presented to the Faculty of the Graduate School of

The University of Texas at Austin

in Partial Fulfillment

of the Requirements

for the Degree of

MASTER OF SCIENCE IN ENGINEERING

THE UNIVERSITY OF TEXAS AT AUSTIN

May 2015

Acknowledgments

I would like to express my deepest gratitude to my supervisor, Prof. Robert W. Heath, Jr. for his valuable insights, constant support and encouragement during the course of this research.

I would especially like to thank my committee member Dr. Philip V. Orlik. Without his priceless advice and support, this work would not have been possible.

I gratefully acknowledge the support of Mitsubishi Electric Research Labs (MERL). I am also thankful to Dr. K. J. Kim and other staff members at MERL for their help and support while I was interning at MERL.

I would also like to thank my friends and colleagues at UT Austin and MERL, particularly my lab mates.

Special thanks to my family members to whom I will ever be indebted.

Last but not least, I would like to thank the Almighty for making all of this possible.

A Stochastic Geometry Analysis of Cooperative Wireless Networks Powered by Energy Harvesting

Talha Ahmed Khan, M.S.E.
The University of Texas at Austin, 2015

Supervisor: Robert W. Heath, Jr.

Energy harvesting technology is essential for enabling green, sustainable and autonomous wireless networks. In this report, a large-scale wireless network with energy harvesting transmitters is considered, where a group of transmitters forms a cluster to cooperatively serve a desired user in the presence of co-channel interference and noise. Using stochastic geometry, simple closed-form expressions are derived to characterize the outage performance at the user as a function of important parameters such as the energy harvesting rate, the energy buffer size and the cluster size for a given cluster geometry. The analysis is further extended to characterize the mean delay due to transmission failure. The developed framework is flexible in that it allows the in-cluster transmitters to have possibly different energy harvesting capabilities. The analytical expressions are first validated using simulations and then used for investigating the impact of different parameters such as cluster and

buffer size on outage performance. The results suggest that substantial outage performance can in fact be extracted with a relatively small energy buffer. Moreover, the utility of having a large energy buffer increases with the cluster size as well as with the energy harvesting rate.

Table of Contents

List of Tables

List of Figures

Chapter 1

Introduction

Advancing energy harvesting technology is essential for enabling a green, sustainable and autonomous wireless network. A wireless device equipped with energy harvesting capability may extract energy from natural or man-made sources such as solar radiations, wind, radio frequency signals, indoor lighting, etc. [22]. For cellular systems, energy harvesting could help reduce the operating expenditures for the cell-sites, as well as facilitate cell-site deployment [7]. Energy harvesting is also closely related to the emerging concept of Internet of Things, which entails an all-pervasive network consisting of everyday objects such as machines, buildings, vehicles, etc [26]. These everyday objects are embedded with low-power wireless sensors that can communicate with other devices such as a control unit. Energy harvesting seems particularly attractive for such scenarios as it can potentially enhance the battery lifetimes while reducing the network maintenance [19, 22].

The main challenge in realizing a self-powered wireless device is two-fold. The first challenge concerns the physical layer, where we need low-power, low-cost and high-efficiency energy conversion circuits. To this end, the semiconductor community has been continually working to advance the state-of-

the-art in energy harvesting devices (see [19, 23] and references therein). The second challenge is related to the communication layer. Due to limited energy storage capacity and depending on the type of harvesting, the energy availability at the device varies over time. Thus, in a self-powered device, not only the data but the energy arrivals could also be bursty. This calls for a rethinking of conventional communication protocols. In this regard, several papers have proposed optimal transmission policies assuming causal or non-causal knowledge about energy arrivals for different setups (see [9, 22] for a comprehensive review). For example, a point-point link [12, 18], an interference channel [21], and a broadcast channel [27] have been considered. While prior research has mostly investigated isolated setups, some recent studies have adopted a stochastic geometry approach to deal with the network-level dynamics in large *non-cooperative* wireless networks powered by energy harvesting [7, 13, 16, 24].

By modeling wireless networks in a stochastic geometry framework, tractable analytical expression can be developed to get general performance insights, thus obviating the need of exhaustive simulations [11]. For this reason, stochastic geometry is emerging as a popular tool for analyzing a variety of setups ranging from ad hoc, to cognitive and cellular networks. Using metrics such as outage probability, transmission capacity and delay, several studies have characterized the performance of an ad hoc network [3, 8, 25]. Similar analysis has been applied to single and multi-tier cellular networks under different assumptions about cell association, scheduling and power con-

trol [2, 6, 8]. Existing models have also been extended to study the benefits of multi-cell cooperation [1, 4, 15, 17, 20]. None of this work, however, considered energy harvesting nodes.

In this report, a large self-powered wireless network is considered where all the transmitters access the medium following a random-access protocol. To reap the benefits of cooperation, they are grouped into clusters such that all the in-cluster transmitters jointly serve a common receiver, which is subjected to interference from out-of-cluster nodes. To the best of our knowledge, the performance of such a *cooperative* self-powered wireless network in a stochastic geometry framework, has not been analyzed. Using stochastic geometry, we derive simple closed-form expressions that characterize the system performance as a function of system parameters (e.g., energy harvesting rate) and cluster geometry, amid interference and noise. The developed framework is flexible in that it allows the in-cluster transmitters to have possibly different energy harvesting capabilities. This analytical model is validated using numerical simulations. The analysis is also extended to characterize the mean delay at the receiver due to transmission failure. In addition, we also investigate the impact of energy harvesting rate and energy buffer size on the outage performance. Our findings suggest that (a) substantial outage performance can in fact be extracted with a relatively small energy buffer size (typically less than 10 in the considered setup); and (b) the utility of having a large energy buffer increases with the cluster size as well as the energy harvesting rate.

A brief overview of stochastic geometry-based work on energy harvesting is in order. The spatial throughput of a large-scale self-powered ad hoc network has been studied [13, 24]. In [13], the network model consists of a large number of energy harvesting transmitters, where each transmitter has a dedicated receiver located a fixed distance away. Leveraging tools from stochastic geometry and random walk theory, spatial throughput was derived by optimizing over the transmission power. For a similar setup, [24] derived the transmission capacity for a random access network by optimizing over the medium access probability. Self-powered heterogeneous cellular networks have been considered in [7]. In [7], base-station availability (i.e., the fraction of the time it can remain ON) was analytically characterized using tools from random walk theory and stochastic geometry. The work in [7, 13, 24], however, does not consider any node cooperation or joint transmission at the physical layer. In contrast, we consider a large-scale network where clusters of self-powered nodes jointly serve a desired user, and provide a tractable framework to characterize the system performance as a function of energy harvesting capability and other network parameters.

In another line of work, stochastic geometry has also been used for modeling cognitive networks with *opportunistic* energy harvesting [16]. The study of large-scale networks with wireless power transfer and simultaneous wireless information and power transfer is yet another related area with considerable research activity (see [14, 22] and references therein). In this report, however, we limit ourselves to a conventional energy harvesting system and

leave the topic of joint information and power transfer for future work.

Chapter 2

System Model

In this chapter, the system model is described in detail beginning with the energy harvesting model. The model parameters are summarized in Table 2.1 for convenience.

2.1 Energy Harvesting Model

We consider a large wireless network consisting of transmitters or access points (APs) that are equipped with energy harvesting modules. None of the transmitters are privy to non-causal information about energy arrivals, which is assumed to be random and independent across nodes. Without loss of generality, we now describe the energy harvesting model for a typical transmitter equipped with an energy buffer of size $S \in \mathbb{N}$. The energy arrives at the buffer with rate ρ following an independent and identically distributed (IID) Bernoulli process, i.e., with probability ρ, one unit of energy arrives at the buffer in time-slot t, while $1 - \rho$ is the probability that no energy arrives at the buffer in that slot. A node may choose to transmit with fixed power P if it has sufficient energy in the buffer. No power control is assumed, therefore each transmission depletes the buffer of P units of energy. The energy arrivals

are modeled using a birth-death Markov process (cf. Fig. 1) along the lines of [13, 24].

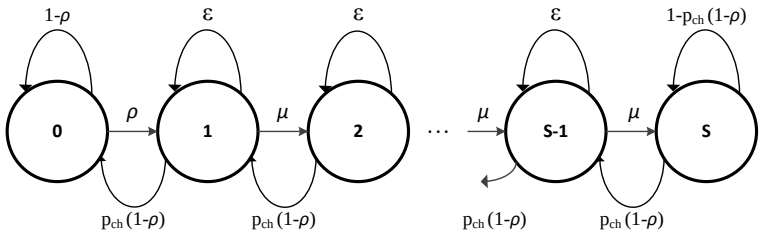

Figure 2.1: Finite-state birth-death Markov chain for an energy buffer of size S with $\mu = \rho(1 - p_{\text{ch}})$ and $\epsilon = \rho p_{\text{ch}} + (1 - \rho)(1 - p_{\text{ch}})$.

For medium access, we consider slotted ALOHA protocol where in each time-slot, a node (having sufficient energy) accesses the medium with probability p_{ch} independently of other nodes. Let $p_S = \Pr\{A_S(t) \geq P\}$, where $A_S(t)$ denotes the state (i.e., energy level) of the buffer at time t. Here, p_S denotes the probability that a node has requisite amount of energy available in the buffer of size S. We now define p_{tr}, the transmission probability of an arbitrary node, and express it as a function of system parameters.

Lemma 2.1.1. *For energy arrivals with rate $\rho > 0$, finite energy buffer of size $S \in \mathbb{N}$, and channel access probability $p_{ch} > 0$, we have $p_{tr} = p_{ch} p_S$ in steady state, where*

$$p_S = \begin{cases} \frac{\rho}{\rho + p_{ch} - \rho p_{ch}} & S = 1 \\ \frac{\frac{\rho}{p_{ch}} \left(1 - \left(\frac{\rho(1-p_{ch})}{p_{ch}(1-\rho)}\right)^S\right)}{1 - \frac{\rho}{p_{ch}} \left(\frac{\rho(1-p_{ch})}{p_{ch}(1-\rho)}\right)^S} & S > 1, \rho \neq p_{ch} \\ \frac{S}{S+1-\rho} & S > 1, \rho = p_{ch}. \end{cases} \tag{2.1}$$

for the case $P = 1$.

Proof. It results from solving the balance equations for the Markov chain shown in Fig. 2.1 (e.g., see [13]). ■

Note that $0 < p_{\text{tr}} \leq p_{\text{ch}}$ since $\lim_{\rho \to 1} p_{\text{tr}} = p_{\text{ch}}$, where $\rho = 1$ corresponds to the case when the node is powered by conventional power sources. Furthermore, we consider p_{ch} to be fixed throughout the network. Therefore, the transmission probability of a node varies as a function of the energy harvesting rate and buffer size. In other words, the higher the p_{tr} of an AP, the more superior the energy harvesting capability (i.e., harvesting rate and/or buffer size). Note that Lemma 1 has been specialized for the case $P = 1$ for simplicity. For other values of P, we can similarly solve the balance equations of the corresponding Markov chain to calculate p_S.

2.2 Network Model

In our setup, a cluster of K cooperating APs jointly serve a desired user over the same time-frequency resource block. It is assumed that each user is served by the K closest APs. The AP locations are drawn from a homogeneous Poisson point process (PPP) of intensity λ, which we denote as $\Phi \triangleq \{d_i, i \in \mathbb{N}\}$. Similarly, the user locations are modeled using another PPP Φ_u of intensity λ_u, which is assumed to be independent of Φ. We further assume that the AP density is sufficiently high relative to the user density such that with a high probability, no two users share the same set of closest APs. Due to concurrent transmissions, the receiver is subjected to co-channel

interference from the out-of-cluster APs. We assume that all out-of-cluster APs contribute to interference. In general, we expect such a network to consist of nodes with different physical parameters (e.g., energy harvesting capability) and random locations (e.g., due to mobility or unplanned deployments). To model this heterogeneous network interference, we consider M additional tiers of nodes, where the nodes in tier m are located according to a homogeneous PPP $\Phi_m \triangleq \{d_{i,m}, i \in \mathbb{N}\}$ of intensity λ_m, independently of other tiers[1]. Note that each class of nodes may differ in terms of energy harvesting rate ρ_m, energy buffer size S_m, and transmit power ${P_m}^2$, etc. All the nodes are assumed to be equipped with a single antenna. Leveraging Slivnyak's theorem [11], we consider a typical user located at origin, and characterize the performance in the presence of co-channel interference and noise.

2.3 Signal Model

All the nodes are assumed to employ orthogonal frequency division multiple access (OFDMA) for communication. We consider a transmission scheme where a group of K cooperating APs jointly transmit the same data to a given user over the same time-frequency resource block. Given the challenges associated with channel acquisition, none of the transmitting APs are

[1]For compactness, we also introduce an alternative notation for the nodes in AP tier Φ. Specifically, the subscript 0 is sometimes used while referring to the quantities of nodes in the AP tier, i.e., $\Phi_0 = \Phi$, $\lambda_0 = \lambda$, etc.

[2]Without loss of generality, we assume the transmit power of the AP tier to be normalized to unity. Therefore, P_m also corresponds to the normalized transmit power of tier m, where the normalization is with respect to the actual transmit power of the AP tier.

Table 2.1: Model Parameters

Notation	**Description**
K	cluster size
η	path-loss exponent
p_{ch}	channel access probability
$p_{\text{tr}} \triangleq 1 - q_{\text{tr}}$	transmission probability
ρ	energy harvesting rate
S	energy buffer size
$\Phi; \lambda$ (or Φ_0, λ_0)	PPP with intensity λ (also denoted as λ_0) modeling AP locations.
$\{p_{\text{tr,i}}\}_{i=1}^{K}$	transmission probabilities of K in-cluster APs in Φ.
$p_{\text{tr},o}$	transmission probability of out-of-cluster APs in Φ.
$\Phi_m; \lambda_m$ $(1 \leq m \leq M)$	PPP with intensity λ_m modeling node locations in tier m.
$p_{\text{tr}}^{(m)}$ $(1 \leq m \leq M)$	transmission probability of nodes in Φ_m.
P_m $(1 \leq m \leq M)$	transmit power of nodes in Φ_m.

assumed to have any instantaneous channel knowledge. The considered joint transmission scheme is simple as it does not require joint encoding at the cooperating transmitters. To further reduce the coordination overhead, we do not assume any tight synchronization among the in-cluster APs. The user, however, is required to know the composite downlink channel from the in-cluster transmitters for coherent detection. The signals transmitted by the cooperating APs superimpose non-coherently at the receiver, resulting in a

received power boost. Moreover, interference seen by the user is treated as noise for the purpose of decoding. The channel model is described next. We define H_i to be the channel power gain for the link from AP i in Φ to the given user. We consider a rich scattering environment where all the links experience IID narrowband Rayleigh fading such that $H_i \sim \exp(1)$. With such a non-coherent joint transmission scheme (see [20, Appendix A] for details), the signal-to-interference-plus-noise ratio (SINR) at the user can be expressed as[3]

$$\gamma \triangleq \frac{\sum_{i=1}^{K} \mathbb{1}_i d_i^{-\eta} H_i}{I + \sigma^2} \tag{2.2}$$

where the indicator function $\mathbb{1}_i$ models the uncertainty due to bursty energy arrivals at the transmitter such that $\Pr\{\mathbb{1}_i = 1\} = p_{\mathrm{tr},i}$ and $\Pr\{\mathbb{1}_i = 0\} = 1 - p_{\mathrm{tr},i} \triangleq q_{\mathrm{tr},i}$ for the in-cluster APs (i.e., $1 \leq i \leq K$), η denotes the pathloss exponent, while σ^2 gives the variance of the receiver noise, which we assume to be zero-mean circularly symmetric complex Gaussian. Moreover, I denotes the aggregate interference power observed at the receiver. It can be expressed as

$$\begin{aligned} I &= I_0 + \sum_{m=1}^{M} I_m \\ &= \underbrace{\sum_{i=K+1}^{\infty} \mathbb{1}_i d_i^{-\eta} H_i}_{\text{intrinsic}} + \underbrace{\sum_{m=1}^{M} \sum_{d_{i,m} \in \Phi_m} \mathbb{1}_{i,m} P_m d_{i,m}^{-\eta} H_{i,m}}_{\text{extrinsic}} . \end{aligned} \tag{2.3}$$

[3]For tractability, it is assumed that the signals transmitted by the interfering APs superimpose non-coherently at the receiver, which would typically be the case.

where the first term I_0 accounts for the (in-network or intrinsic) interference from the out-of-cluster APs belonging to Φ. Here, $\Pr\{\mathbb{1}_i = 1\} = p_{\mathrm{tr},o}$ while $\Pr\{\mathbb{1}_i = 0\} = 1 - p_{\mathrm{tr},o} \triangleq q_{\mathrm{tr},o}$ for all the out-of-cluster APs (i.e., $i > K$). The second term $\sum_{m=1}^{M} I_m$ models the (out-of-network or extrinsic) interference from the nodes belonging to the M interfering tiers $\{\Phi_m\}_{m=1}^{M}$. Note that for the interfering tiers, we use a slightly modified notation by including i, m in the subscript to denote a node i that belongs to the interfering tier Φ_m. As done for the AP tier Φ, we can similarly define $\Pr\{\mathbb{1}_{i,m} = 1\} = p_{\mathrm{tr}}^{(m)}$ for the nodes in tier m. The assumptions about the channel model are as explained for the AP tier Φ, i.e., $H_{i,m} \sim \exp(1)$.

Notation. Table 2.1 summarizes the notation introduced in this section. We adopt the following notation for the transmission probabilities of the nodes belonging to tier Φ. For $i = 1, \cdots, K$, we define $p_{\mathrm{tr},i} \triangleq 1 - q_{\mathrm{tr},i}$ to be the transmission probability of the i^{th} in-cluster AP belonging to Φ, whereas $p_{\mathrm{tr},o}$ gives the transmission probability of all other (i.e., out-of-cluster) APs in Φ. Similarly, for $m = 1, \cdots, M$ we define $p_{\mathrm{tr}}^{(m)} \triangleq 1 - q_{\mathrm{tr}}^{(m)}$ to be the transmission probability of the nodes belonging to the interfering tier Φ_m. The above notation allows both the in-cluster and out-of-cluster nodes to have different transmission probabilities. This is in line with the considered model, where we have allowed the nodes to have possibly different energy harvesting capabilities. For ease of exposition, we define $\Xi = \left[q_{\mathrm{tr},i}, \cdots, q_{\mathrm{tr},K}, q_{\mathrm{tr},o}, q_{\mathrm{tr}}^{(1)}, \cdots, q_{\mathrm{tr}}^{(M)}\right]$, which depends on the energy harvesting parameters (i.e., energy harvesting

rate and energy buffer size). We also define

$$Q = \prod_{i=1}^{K} q_{\mathrm{tr},i}. \tag{2.4}$$

For the APs (in Φ) belonging to a cluster of size K, we define $\omega_i = \frac{d_i}{d_K}$ such that $\{\omega_i\}_{i=1}^{K}$ denotes a set of normalized distances. This set is assumed to be arranged in ascending order, i.e., d_1 refers to the closest serving AP while d_K refers to the AP located farthest away from the user. We also define $\Omega = \{\omega_1^{\eta}, \cdots, \omega_K^{\eta}\}$, $\hat{\Omega} = \{\frac{\omega_1^{\eta}}{q_{\mathrm{tr},1}}, \cdots, \frac{\omega_K^{\eta}}{q_{\mathrm{tr},K}}\}$ and

$$\alpha_i(\Omega) = (-1)^i \overset{+}{\sum} \left[\binom{K}{K-i}_{\Omega} \right] \tag{2.5}$$

where $\overset{+}{\sum}[\cdot]$ gives the sum of the elements of the set that it operates on. With a slight abuse of notation, $\binom{K}{K-i}_{\Omega}$ is defined to be the set of all products of the elements of Ω taken $K-i$ at a time. The summation in (2.5) is taken over the elements of the set $\binom{K}{K-i}_{\Omega}$. Similarly, the definition of $\alpha_i(\hat{\Omega})$ follows from (2.5) with the set Ω now replaced by $\hat{\Omega}$. For the intensity parameters, we define $\Lambda = [\lambda_0, \cdots, \lambda_m]$ (recall that $\lambda_0 = \lambda$ gives the intensity of the PPP $\Phi_0 = \Phi$).

Chapter 3

Stochastic Geometry Analysis

In this chapter, closed-form expressions are provided for the coverage probability and mean delay at a typical user using tools from stochastic geometry.

3.1 Coverage Analysis

The following theorem gives a closed-form expressions for the complementary cumulative distribution function (CCDF) of γ (or equivalently the coverage probability) at a receiver, as a function of network parameters and cluster geometry.

Theorem 3.1.1. *For a cluster of size K, the CCDF of γ, $\bar{F}_{\gamma}(K,\theta) = \Pr\{\gamma > \theta\}$, can be expressed in terms of the interference intensity parameters (Λ), noise power (σ^2), energy harvesting parameters (Ξ) and cluster geometry $\left(\{d_i\}_{i=1}^{K}\right)$ as*

$$\bar{F}_{\gamma}(K,\theta) = Q \sum_{j=1}^{K} \left(\frac{\sum_{i=0}^{K-1} \left(\alpha_i(\hat{\Omega}) - \alpha_i(\Omega)\right) (\omega_j^{\eta})^i}{\omega_j^{\eta} \left(\prod_{l \neq j}^{K} \omega_l^{\eta} - \omega_j^{\eta} \right)} \right) \Delta_j(\theta) \tag{3.1}$$

where

$$\Delta_j(\theta) = e^{-d_j^{\eta}\theta\sigma^2} e^{-\pi p_{tr,o}\lambda d_K^2 \mathcal{F}\left(\omega_j^{\eta}\theta,\eta\right)} \Psi_j\left(M\right) \tag{3.2}$$

with

$$\Psi_j\left(M\right) = \prod_{m=1}^{M} e^{-\pi p_{tr}^{(m)}\lambda_m {d_j}^2 (\theta P_m)^{\frac{2}{\eta}} \Gamma\left(1+\frac{2}{\eta}\right)\Gamma\left(1-\frac{2}{\eta}\right)} \tag{3.3}$$

and

$$\mathcal{F}\left(U,V\right) = \frac{2U}{V-2} {}_2F_1\left(1, 1-\frac{2}{V}, 2-\frac{2}{V}, -U\right) \tag{3.4}$$

where ${}_2F_1(\cdot)$ *is the Gauss hypergeometric function.*

Proof. See Appendix A. ■

Remark 3.1.1. Note that Theorem 3.1.1 allows the in-cluster APs to have possibly different energy harvesting rates and/or energy buffer sizes, and is therefore useful for getting general insights about the performance when the cluster consists of heterogeneous APs. Similarly, the multi-tier approach allows us to capture the heterogeneity in out-of-cluster nodes. Furthermore, all the interfering APs can be assumed to have the maximum harvesting rate/buffer size in order to get a lower bound on performance.

Some special cases of Theorem 3.1.1 are listed below.

- $\theta \to 0$. In the low-outage regime, the performance is dominated by the energy harvesting parameters and the cluster size. In particular, as

$\theta \to 0$ in (3.1), we get $\lim_{\theta \to 0} \bar{F}_{\gamma}(K, \theta) = 1 - Q$, where Q defines a limit on the performance and infact represents the exact outage probability in the asymptotic regime. This observation also holds for Theorem 3.1.2.

- $\{q_{\mathrm{tr},i}\}_{i=1}^{K} = q_{\mathrm{tr},o} \triangleq q_{\mathrm{tr}}$. When all the APs in Φ have identical energy harvesting capabilities, i.e., $q_{\mathrm{tr},i} = q_{\mathrm{tr},o} \triangleq q_{\mathrm{tr}}$, the CCDF in (3.1) simplifies to

$$\bar{F}_{\gamma}(K, \theta) = \sum_{j=1}^{K} \left(\frac{\sum_{i=0}^{K-1} \alpha_i(\Omega) \left({q_{\mathrm{tr}}}^{i} - {q_{\mathrm{tr}}}^{K} \right) (\omega_j^{\eta})^i}{\omega_j^{\eta} \left(\prod_{l \neq j}^{K} \omega_l^{\eta} - \omega_j^{\eta} \right)} \right) \Delta_j(\theta) \tag{3.5}$$

  where $\Delta_j(\theta)$ is given by (3.2).

Note that Theorem 3.1.1 can be used for analyzing cooperative setups in the presence of interference and noise, for a given cluster geometry. For a network consisting of homogeneous APs, we provide a more general result in terms of normalized distances by unconditioning w.r.t. d_K.

Theorem 3.1.2. *In the interference-limited regime ($\sigma^2 \to 0$), the CCDF of γ, $\bar{F}'_{\gamma}(K, \theta)$, can be expressed as a function of cluster size K, interference intensity parameters Λ and energy harvesting parameters Ξ for a normalized*

cluster geometry $\{\omega_i\}_{i=1}^{K}$ *as* [1]

$$\bar{F}'_{\gamma}(K,\theta) = \sum_{j=1}^{K} \left(\frac{\sum_{i=0}^{K-1} \alpha_i(\Omega) \left({q_{tr}}^{i} - {q_{tr}}^{K} \right) (\omega_j^{\eta})^i}{\omega_j^{\eta} \left(\prod_{l \neq j}^{K} \omega_l^{\eta} - \omega_j^{\eta} \right)} \right) \varpi_j(\theta) \tag{3.6}$$

where

$$\varpi_j(\theta) = \left(1 + \mathcal{F}\left(\omega_j^{\eta}\theta, \eta\right) + \Upsilon_j(M)\right)^{-K} \tag{3.7}$$

and

$$\Upsilon_j(M) = {\omega_j}^2 \theta^{\frac{2}{\eta}} \Gamma\left(1 + \frac{2}{\eta}\right) \Gamma\left(1 - \frac{2}{\eta}\right) \sum_{m=1}^{M} \tilde{p}_{tr}^{(m)} \tilde{\lambda}_m {P_m}^{\frac{2}{\eta}} \tag{3.8}$$

with $\tilde{p}_{tr}^{(m)} = \frac{p_{tr}^{(m)}}{p_{tr}}$ *and* $\tilde{\lambda}_m = \frac{\tilde{\lambda}_m}{\lambda}$.

Proof. See Appendix B. ■

Remark 3.1.2. For the case with no extrinsic interference, i.e., with the M interfering tiers turned off, the CCDF expression in Theorem 3.1.2 is independent of the AP intensity λ. This is because the probability of finding the closest AP around the receiver increases with λ, but so does the interference such that the two effects cancel out.

Remark 3.1.3. With the M interfering tiers now turned on, the CCDF expression in Theorem 3.1.2 is no longer independent of the intensity parameters

[1] Here, the superscript $'$ is used in $\bar{F}'_{\gamma}(K,\theta)$ to differentiate it from the earlier notation $\bar{F}_{\gamma}(K,\theta)$ used for Theorem 1.

Λ. In this case, increasing the AP intensity λ (or more generally the effective intensity $p_{\text{tr}}\lambda$) helps dilute the intensity of the interfering tiers. This is supported by (3.8) where the term inside the summation vanishes as λ is increased. This neutralizes the harmful term $\Upsilon_j(M)$, which captures the effect of extrinsic interference. This is in contrast to the previous case where the AP intensity λ played no role.

Some more special cases are postulated below assuming the M tiers to be turned off.

- $p_{\text{tr}} \to 1$. It is worth noting that without energy harvesting and a random medium access protocol, i.e., as $p_{\text{tr}} \to 1$ in (3.6), and further assuming the M interfering tiers to be turned off, we can retrieve the expression for the CCDF of γ in a traditionally powered cooperative network as given in [15], which Theorem 3.1.2 generalizes.

- $K = 1$. For the non-cooperative case, the expression in (3.6) simplifies to $\bar{F}'_{\gamma}(1,\theta) = (1-q_{\text{tr}})(1+\mathcal{F}(\theta,\eta))^{-1}$. Furthermore, with $q_{\text{tr}} = 0$, we can retrieve the CCDF expression for the signal-to-interference ratio (SIR) in a traditionally powered non-cooperative network as given in [2].

This shows that our analytical framework is fairly general with the traditional cooperative and non-cooperative networks as special cases.

3.2 Delay Characterization

In this section, we characterize the mean delay seen by a successful packet reception at the typical user as a function of network parameters and cluster geometry. We use T to denote the number of successive transmission attempts (or time-slots) before a packet is successfully received at the typical user. A successful packet reception in an attempt i is denoted by $\mathcal{E}_i$, whereas $\bar{\mathcal{E}}_i$ denotes the corresponding outage event. To characterize the delay, consider

$$\begin{aligned}\Pr\{T=n\} &= \Pr\{\bar{\mathcal{E}}_1,\cdots,\bar{\mathcal{E}}_{n-1},\mathcal{E}_n\}\\ &= \Pr\{\gamma_1\leq\theta,\cdots,\gamma_{n-1}\leq\theta,\gamma_n>\theta\}\\ &= \Pr\{\gamma_n>\theta\}\prod_{i=1}^{n-1}\left(1-\Pr\{\gamma_i>\theta\}\right) \qquad (3.9)\end{aligned}$$

where γ_i denotes the SINR observed in time-slot i, as given in (2.2). The last equation follows due to the IID assumption on fading, and by further assuming the PPP realizations to be independent across slots, which would be the case in a highly mobile environment. Note that if the interferer locations are assumed to be static, the average delay would be higher due to correlated interference as noted in [5] (therefore, in the considered setup, $\mathbb{E}[T]$ can be interpreted as a lower bound on the actual mean delay). Furthermore, the term $\Pr\{\gamma_i>\theta\}$ is independent of i, and is given by Theorem 3.1.1 (or Theorem 3.1.2). Under these assumptions, T can be treated as a geometric random variable with parameter $\Pr\{\gamma>\theta\}$. Therefore, the mean of T can be expressed as

$$\mathbb{E}[T]=\frac{1}{\bar{F}_\gamma(K,\theta)} \qquad (3.10)$$

where $\bar{F}_\gamma(K,\theta)$ is given by (3.1). Similarly we can express the variance of T as

$$\mathrm{Var}[T] = \frac{F_\gamma(K,\theta)}{\bar{F}_\gamma(K,\theta)^2}. \tag{3.11}$$

Similarly, by replacing $\bar{F}_\gamma(K,\theta)$ with $\bar{F}'_\gamma(K,\theta)$ using (3.6), we can extend the above result to the scenario discussed in Theorem 3.1.2.

Chapter 4

Simulation Results

In this chapter, we validate the analytical model using numerical simulations. Moreover, we also investigate the impact of several parameters on outage performance.

4.1 Coverage Results

We first consider the case with heterogeneous in-cluster APs, and plot $\bar{F}_{\gamma}(K, \theta)$, the CCDF of γ, for various values of K in Fig. 4.1. The analytical (anlt) CCDF is based on Theorem 3.1.1, while the simulated (sim) curve is obtained by Monte Carlo simulations for the given set of parameters. The analytical model is validated since there is a complete agreement between analytical and simulation results. Moreover, we can also observe that the SINR distribution at the receiver improves with K due to an additional transmit diversity gain. Also, the outage performance is limited by the energy harvesting capabilities as the CCDF converges to $1 - Q$ in the low-outage regime ($\theta \to 0$) for any given cluster.

We now consider the case discussed in Theorem 3.1.2, where the APs have identical energy harvesting capabilities. In Fig. 3, we plot $\bar{F}'_{\gamma}(K, \theta)$, the

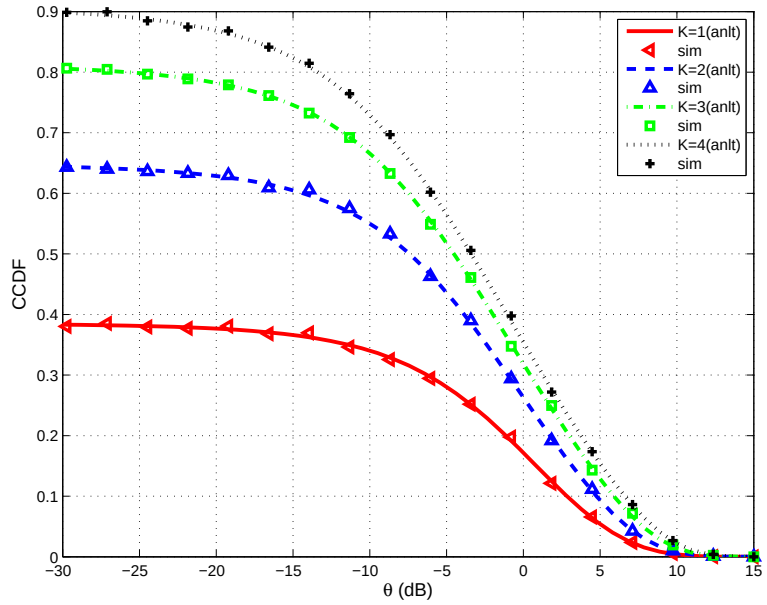

Figure 4.1: CCDF of γ for various values of K given $p_{\text{ch}} = 0.7, \lambda = 0.1, \sigma^2 = 0.01, \eta = 4$ and $\{d_i\}_{i=1}^4 = \{2, 3, 4, 5\}$. The plot is obtained for a single interfering tier $M = 1$ with $\lambda_1 = 0.01$, $p_{\text{tr}}^{(1)} = 0.53$ and $P_1 = 2$. Energy harvesting parameters for the AP tier are $\{\rho_i\}_{i=1}^4 = \{0.4, 0.45, 0.5, 0.55\}$, $\rho_o = 0.55$ and $S = 2$. Simulation (sim) results agree with the analytical (anlt) results based on Theorem 3.1.1.

CCDF of γ with the absolute in-cluster distances averaged out. The plot in Fig. 4.2a is obtained with the interfering tiers turned off. Note that the intensity parameter is not specified as the performance is independent of λ for this case. It can be seen that there is a complete match between the analytical curve based on Theorem 3.1.2 and the simulated CCDF obtained via Monte Carlo simulations. A complete match between analytical and simulation results can also be observed in Fig. 4.2b, which is obtained with the interfering tiers turned on.

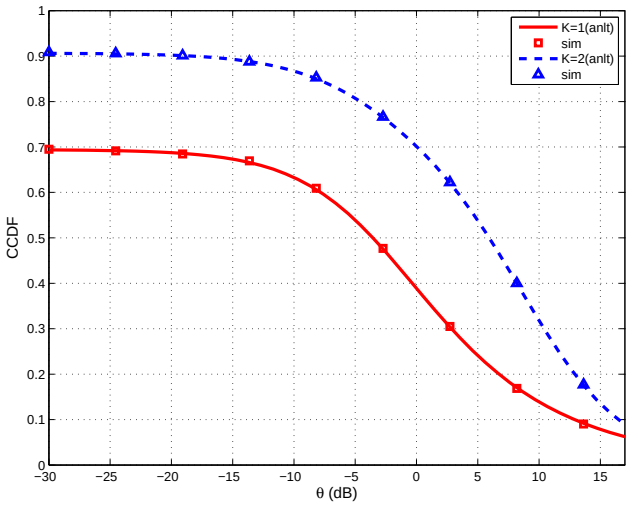

(a)

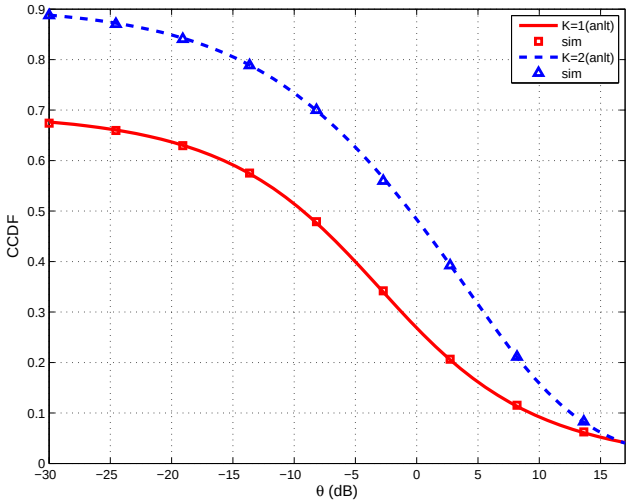

(b)

Figure 4.2: (a) CCDF of γ in the interference-limited regime for $K \in \{1, 2\}$ with the M tiers turned off (i.e., intrinsic interference only). The plot includes the analytical (anlt) curve based on Theorem 3.1.2 as well as the simulated (sim) CCDF of γ. The simulation parameters are $\omega_1 = 1$ for $K = 1$ and $\{\omega_i\}_{i=1}^{2} = \{0.5, 1\}$ for $K = 2$, $p_{\text{ch}} = 0.8$ and $\eta = 4$. The energy harvesting parameters are $\rho = 0.75$ and $S = 2$ for all APs. (b) For the same parameters, CCDF of γ now plotted when both intrinsic and extrinsic interference are present. Other parameters include $M = 1$, $P_1 = 2$, and $p_{\text{tr}}^{(1)} = 0.5$. Unlike (a) which is independent of intensity, (b) is obtained for $\lambda = 0.1$ and $\lambda_1 = 0.05$.

4.2 Delay Results

Having validated the model, we plot the average delay $\mathbb{E}[T]$ experienced by a typical packet against the outage threshold θ for the interference-limited case addressed in Theorem 3.1.2 (Fig. 4.3a). Note that this result does not correspond to a particular realization of the in-cluster AP locations. Rather, it is averaged over all AP realizations that share the same in-cluster geometry. In this example, we consider the case when the neighboring APs are equidistant, i.e., $\{\omega_i\}_{i=1}^{K} = \{\frac{i}{K}\}_{i=1}^{K}$ for a given K. In Fig. 4.3b, the coefficient of variation of T (given by $\frac{\sqrt{\mathrm{Var}[T]}}{\mathbb{E}[T]}$) is also plotted. The coefficient of variation is relatively small in the medium-low outage regime, particularly for large K. This suggests that the average delay is representative of the actual T seen by most packets. Similar plots can also be obtained for the setup addressed in Theorem 3.1.1.

As demonstrated above, the considered framework can be used to get general performance insights for a large class of self-powered wireless networks. We next study how the energy harvesting parameters impact the outage performance.

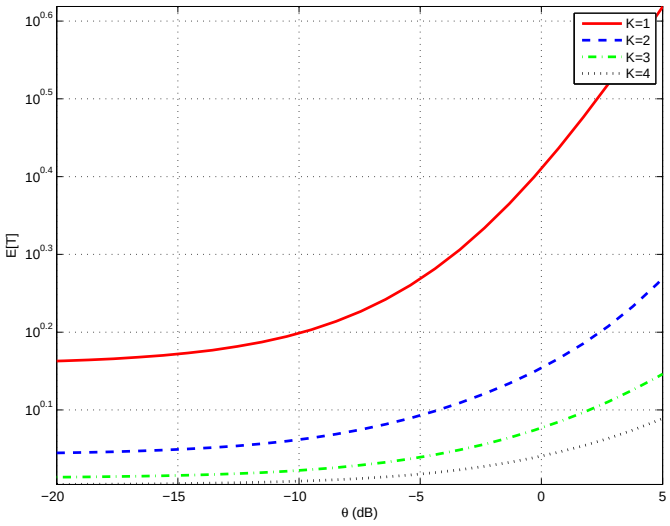

(a)

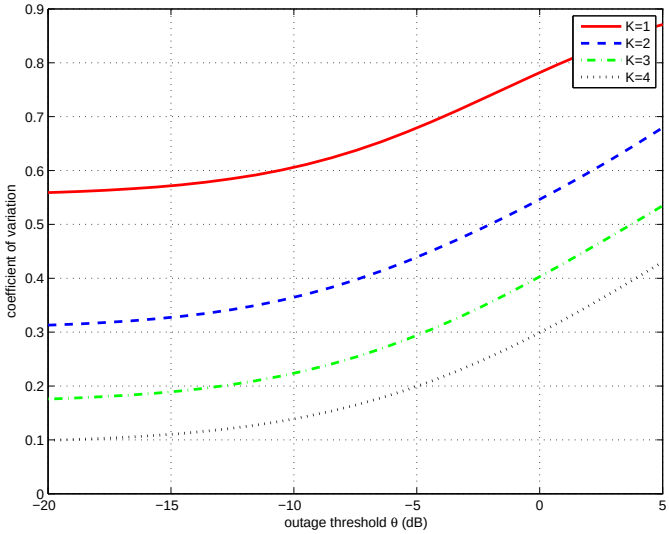

(b)

Figure 4.3: (a) Plots the mean delay $\mathbb{E}[T]$ vs. outage threshold θ in the interference-limited regime for cluster size $K \in \{1, 2, 3, 4\}$ with the in-cluster geometry $\{\omega_i\}_{i=1}^{K} = \{\frac{i}{K}\}$, channel access probability $p_{\text{ch}} = 0.8$ and path loss exponent $\eta = 4$. The energy harvesting parameters are $\rho = 0.75$ and $S = 2$ for all APs. (b) Plots the coefficient of variation $\frac{\sqrt{\text{Var}[T]}}{\mathbb{E}[T]} \in (0, 1)$ for the delay metric. A lower coefficient of variation indicates that the corresponding mean delay is more representative of the delay seen by most packets.

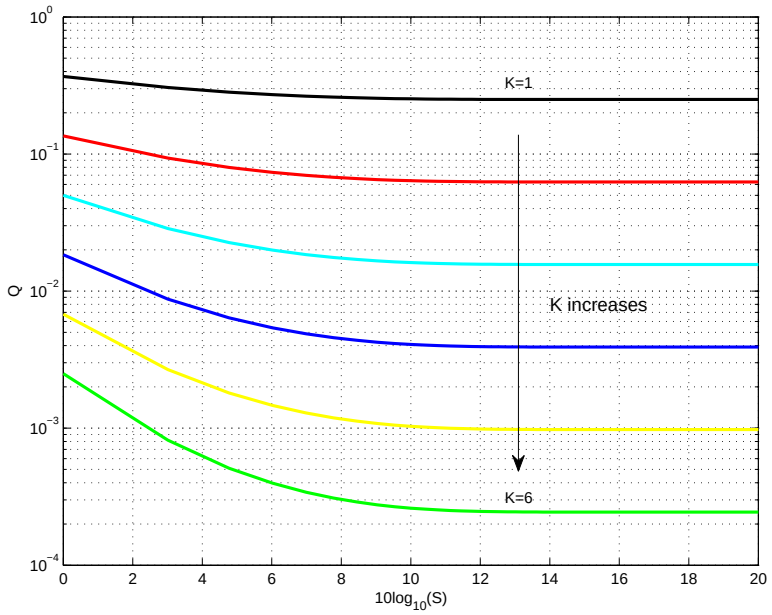

Figure 4.4: Impact of energy buffer size S on asymptotic outage probability Q for various values of K at fixed $\rho = 0.75$ and $p_{\text{ch}} = 0.8$.

4.3 Impact of energy buffer size on performance

In Fig. 4.4, the asymptotic outage probability Q[1] is plotted against the energy buffer size S (in log scale) for various values of the cluster size K. It can be seen that outage can be considerably reduced by increasing the buffer size until a limit, beyond which the curves tend to flatten out. It appears that appreciable performance gains can be extracted with a relatively small buffer size. Moreover, the benefits of having a high-capacity buffer tends to increase with the cluster size as depicted by the increasing steepness of the

[1]It is possible to particularize the analysis for a given outage threshold θ. However, to get general performance insights, we use Q, which also defines a lower limit on the outage probability given the energy harvesting parameters.

slopes (when S is small) as K is increased. This interplay between cluster and buffer size also suggests that the extent of cooperation could influence the design of energy harvesting devices, even though the energy harvesting process is assumed to be independent across the cooperating APs. In addition, we can also observe that the outage is reduced by roughly an order of magnitude with every addition in the cluster size.

4.4 Impact of energy harvesting rate on performance

In Fig. 4.5, the asymptotic outage probability Q is plotted against the energy harvesting rate ρ for various values of energy buffer size S. It can be seen that outage reduces with the increase in energy harvesting rate at the transmitters. Moreover, using a larger energy buffer brings about further reduction in outage due to enhanced energy availability at the transmitters. Furthermore, the gains from using a larger buffer size are more evident at relatively high energy harvesting rates. Fig. 4.5 also corroborates the previous observation (cf. Fig. 4.4) that substantial performance can be extracted by using a relatively small buffer size. For example, $S = 10$ suffices for this setup. In addition, if the energy harvesting rate ρ exceeds the channel access probability p_{ch}, and the buffer size is allowed to increase, the outage performance limit becomes independent of the energy harvesting rate ρ. This is because under these conditions, the energy harvesting system tends to behave like a traditionally powered system.

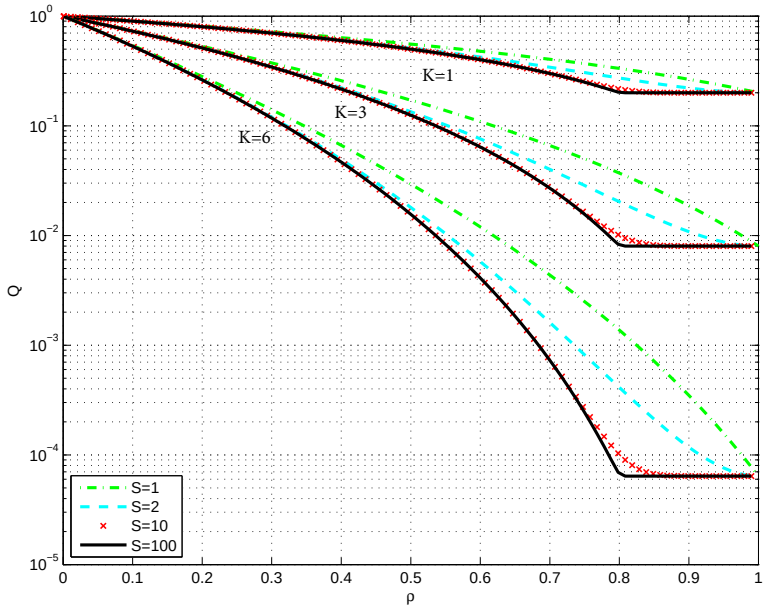

Figure 4.5: Impact of energy harvesting rate ρ on asymptotic outage probability Q for various values of energy buffer size S at fixed $p_{\text{ch}} = 0.8$. The curves are plotted for cluster size $K \in \{1, 3, 6\}$.

Chapter 5

Conclusion

We have derived closed-form expressions to characterize the outage performance at a receiver, in a self-powered clustered wireless network, in the presence of interference and noise. The developed framework is applicable to a general class of networks, with the traditional cooperative and non-cooperative networks as special cases. It can be used to get general performance insights even when the in-cluster nodes have different energy harvesting capabilities. Moreover, we have also investigated the impact of in-cluster energy harvesting parameters on performance. Simulation results reveal that the outage performance improves with the buffer size and the energy harvesting rate. Furthermore, most performance gains can be extracted using a relatively small buffer size, with the improvement becoming more pronounced for large clusters.

Appendices

Appendix A

Proof of Theorem 1

Using (2.2), we have $\bar{F}_{\gamma}\left(K,\theta\right)=\Pr\{\gamma>\theta\}=\mathbb{E}\left[\Pr\left\{S_K>\theta d_K^{\eta}\left(I+\sigma^2\right)\right\}\right]$ where $S_K=\sum_{i=1}^{K}\mathbb{1}_i\hat{H}_i$ and $\hat{H}_i=H_i\omega_i^{-\eta}$. To proceed further, we first find the CCDF of S_K, where S_K is a sum of K independent random variables. Note that $\hat{H}_i$ is exponentially distributed with mean $\omega_i^{-\eta}$, whereas the indicator function follows a Bernoulli distribution with mean $p_{\mathrm{tr},i}$, independent of $\hat{H}_i$. Using the result from Theorem C.1.1 (Appendix C), the CCDF of S_K can be expressed as $(x\geq 0)$

$$\bar{F}_{S_k}\left(x\right)=Q\sum_{j=1}^{K}\left(\frac{\sum_{i=0}^{K-1}\left(\alpha_i(\hat{\Omega})-\alpha_i(\Omega)\right)\left(\omega_j^{\eta}\right)^i}{\omega_j^{\eta}\left(\prod_{l\neq j}^{K}\omega_l^{\eta}-\omega_j^{\eta}\right)}\right)e^{-\omega_j^{\eta}x} \tag{A.1}$$

Conditioning on the aggregate interference power I, we can write $\bar{F}_{\gamma|I}\left(K,\theta\right)=\bar{F}_{S_K}\left(\theta d_K^{\eta}(I+\sigma^2)\right)$. Using (A.1), and unconditioning w.r.t. I, we can express $\bar{F}_{\gamma}\left(K,\theta\right)$ (for $\theta\geq 0$) as

$$\bar{F}_{\gamma}(K,\theta)=Q\sum_{j=1}^{K}\left(\frac{\sum_{i=0}^{K-1}\left(\alpha_i(\hat{\Omega})-\alpha_i(\Omega)\right)\left(\omega_j^{\eta}\right)^i}{\omega_j^{\eta}\left(\prod_{l\neq j}^{K}\omega_l^{\eta}-\omega_j^{\eta}\right)}\right)\mathbb{E}\left[e^{-\omega_j^{\eta}d_K^{\eta}\theta\left(I+\sigma^2\right)}\right] \tag{A.2}$$

where the expectation in $(A.2)$ is over the aggregate interference power I, i.e., over both fading and interferer locations. We next find the expectation of the term $\mathbb{E}\left[e^{-d_j{}^{\eta}\theta(I+\sigma^2)}\right] = e^{-d_j{}^{\eta}\theta\sigma^2}\mathbb{E}\left[e^{-d_j{}^{\eta}\theta I}\right]$. Since the PPPs $\{\Phi_m\}_{m=0}^{M}$ are assumed to be independent, we have

$$\mathbb{E}\left[e^{-d_j{}^{\eta}\theta I}\right] = \mathbb{E}\left[e^{-d_j^{\eta}\theta I_0}\right]\prod_{m=1}^{M}\mathbb{E}\left[e^{-d_j^{\eta}\theta I_m}\right] \tag{A.3}$$

where the first term (with $m = 0$) corresponds to intrinsic interference, whereas the remaining terms ($m \geq 1$) correspond to extrinsic interference. The expectation in (A.3) can be evaluated using the Laplace transform of I_m, which we denote by $\mathcal{L}_{I_m}(s) = \mathbb{E}\left[e^{-sI_m}\right]$.

$$\begin{aligned}
\mathcal{L}_{I_m}(s) &= \mathbb{E}\left[e^{-s\left(\sum\limits_{d_i\in\Phi_m\setminus\mathcal{B}(g_m)} P_m\mathbb{1}_i H_i d_i^{-\eta}\right)}\right] \\
&\overset{(a)}{=} \mathbb{E}\left[\prod_{d_i\in\hat{\Phi}_m\setminus\mathcal{B}(g_m)} \mathrm{E}\left[e^{-sP_m H_i d_i^{-\eta}}\right]\right] \\
&\overset{(b)}{=} \mathbb{E}\left[\prod_{d_i\in\hat{\Phi}_m\setminus\mathcal{B}(g_m)} \frac{1}{1+sP_m d_i^{-\eta}}\right] \\
&= \exp\left(-2\pi\hat{\lambda}_m\int_{g_m}^{\infty}\frac{x}{1+s^{-1}{P_m}^{-1}x^{\eta}}\mathrm{d}x\right)
\end{aligned} \tag{A.4}$$

where $\mathcal{B}(g_m)$ denotes a disc of radius g_m centered at origin, and is used to model an interference-free guard zone around the user w.r.t. tier m. The inner expectation in (a) is over fading power while the outer expectation is over the PPP Φ_m of intensity λ_m outside $\mathcal{B}(g_m)$. Next, we exploit the property of independent thinning of a PPP to deal with the transmission indicator

and consider a (thinned) PPP $\hat{\Phi}_m$ with effective density $\hat{\lambda}_m = p_{\mathrm{tr}}^{(m)}\lambda_m$ for $1 \leq m \leq M$ and $\hat{\lambda}_m = p_{\mathrm{tr,o}}\lambda_m$ for $m = 0$. As the fading is i.i.d. across links and from further conditioning over the location, we obtain (b). The last equation follows by invoking the probability generating functional (PGFL) [11] of the PPP and further algebraic manipulations. With additional algebraic steps, (A.4) can be expressed in terms of hypergeometric function, which with $s = d_j^{\eta}\theta$, gives

$$\mathcal{L}_{I_m}(s)|_{s=d_j^{\eta}\theta} = \exp\left(-\pi\hat{\lambda}_m g_m^2 \mathcal{F}\left(\frac{d_j^{\eta}}{g_m^{\eta}}P_m\theta, \eta\right)\right) \tag{A.5}$$

where $\mathcal{F}(\cdot,\cdot)$ is given by (3.4). To compute the expectation of the term in (A.3) arising due to out-of-cluster APs in Φ_0, we set $g_0 = d_K$. This is because the cluster is assumed to consist of the K closest nodes and interference is due to the nodes located outside this protection zone. For the interfering tiers $\{\Phi_m\}_{m=1}^{M}$, however, we have not assumed any protection zone around the receiver. With no interference-free protection zone (i.e., $g_m \to 0$), $\mathcal{L}_{I_m}(s)$ further simplifies to

$$\mathcal{L}_{I_m}(s)|_{s=d_j^{\eta}\theta} = \exp\left(-\pi\hat{\lambda}_m {d_j}^2\Gamma(1+2/\eta)\Gamma(1-2/\eta)(P_m\theta)^{2/\eta}\right) \tag{A.6}$$

where $\Gamma(\cdot)$ is the Gamma function [11]. Evaluating the expectation in (A.2) using (A.5), (A.6), and further substituting $P_0 = 1$, $\hat{\lambda}_0 = p_{\mathrm{tr},o}\lambda_0$, $\hat{\lambda}_m = p_{\mathrm{tr}}^{(m)}\lambda_m$ and $d_j = \omega_j d_K$, we obtain the result in Theorem 1. ■

Appendix B

Proof of Theorem 2

We begin the proof along the lines of [15] by leveraging a known result on PPP distance distribution. As shown in [10], the distance d_K, between a typical user and its K^{th} closest AP, follows a generalized Gamma distribution, i.e.,

$$f_{d_K}(r) = 2(r\Gamma(K))^{-1}(p_{\text{tr}}\lambda\pi r^2)^K e^{-p_{\text{tr}}\lambda\pi r^2} \tag{B.1}$$

where $\Gamma(K)$ is the Gamma function. Plugging $\sigma^2 = 0$ in (3.2), and taking expectation w.r.t. d_K, we have

$$\begin{aligned}
&\mathbb{E}\left[\Delta_j(\theta)\right] = \\
&\int_{r>0} e^{-\pi p_{\text{tr}}\lambda r^2 \mathcal{F}\left(\omega_j^{\eta}\theta,\eta\right)} \prod_{m=1}^{M} e^{-\pi p_{\text{tr}}^{(m)}\lambda_m {\omega_j}^2 (P_m\theta)^{\frac{2}{\eta}}\Gamma\left(1+\frac{2}{\eta}\right)\Gamma\left(1-\frac{2}{\eta}\right)} \frac{2(p_{\text{tr}}\lambda\pi r^2)^K e^{-p_{\text{tr}}\lambda\pi r^2}}{r\Gamma(K)}\mathrm{d}r \\
&= \int_0^{\infty} \frac{e^{-\upsilon}\upsilon^{K-1}}{\Gamma(K)\left(1+\mathcal{F}\left(\omega_j^{\eta}\theta,\eta\right)+{\omega_j}^2\theta^{\frac{2}{\eta}}\Gamma\left(1+\frac{2}{\eta}\right)\Gamma\left(1-\frac{2}{\eta}\right)\sum_{m=1}^{M}\tilde{p}_{\text{tr}}^{(m)}\tilde{\lambda}_m {P_m}^{\frac{2}{\eta}}\right)^K}\mathrm{d}\upsilon \\
&= \frac{1}{\left(1+\mathcal{F}\left(\omega_j^{\eta}\theta,\eta\right)+{\omega_j}^2\theta^{\frac{2}{\eta}}\Gamma\left(1+\frac{2}{\eta}\right)\Gamma\left(1-\frac{2}{\eta}\right)\sum_{m=1}^{M}\tilde{p}_{\text{tr}}^{(m)}\tilde{\lambda}_m {P_m}^{\frac{2}{\eta}}\right)^K}
\end{aligned} \tag{B.2}$$

where the last equation is obtained by using a dummy variable

$$\upsilon = \pi r^2 \left(p_{\text{tr}} \lambda \left(1 + \mathcal{F}\left(\omega_j^{\eta} \theta, \eta \right) \right) + {\omega_j}^2 \theta^{\frac{2}{\eta}} \Gamma\left(1 + \frac{2}{\eta} \right) \Gamma\left(1 - \frac{2}{\eta} \right) \sum_{m=1}^{M} \tilde{p}_{\text{tr}}^{(m)} \tilde{\lambda}_m {P_m}^{\frac{2}{\eta}} \right) \tag{B.3}$$

for integration, and then applying the definition of the Gamma function $\Gamma(K) = \int_0^{\infty} e^{-x} x^{K-1} \mathrm{d}x$. By taking expectation of (3.5) w.r.t. d_K, and using (B.2), we recover the expression in Theorem 2. ■

Appendix C

Sum of Bernoulli-weighted Exponentials

This appendix is self-contained in terms of the notation used. Moreover, the variables used stating the results in this appendix should not be confused with those introduced elsewhere in this report.

C.1 Main Result

Consider a sum of K independent bernoulli-weighted exponential random variables $\left(\{\epsilon_i\}_{i=1}^K\right)$ such that $S_K = \sum_{i=1}^{K} \epsilon_i$ with $\epsilon_i \triangleq z_i G_i$. Here, $z_i \sim \text{Bern}(p_i)$, $p_i \triangleq 1 - q_i$ and independent across i. Note that we do not require $\{z_i\}_{i=1}^K$ to have distinct means. Independently of $\{z_i\}_{i=1}^K$, we define independent random variables $\{G_i\}_{i=1}^k$ such that $G_i \sim \exp(\lambda_i)$, $\Lambda \triangleq [\lambda_1, \cdots, \lambda_K]$, and Λ has τ unique entries[1]. Note that $1 \leq \tau \leq K$, where $\tau = 1$ when λ_i are equal and $\tau = K$ when λ_i are distinct. We further define $\{\delta_i\}_{i=1}^{\tau}$ to be the set of all unique elements of Λ, where δ_i has multiplicity r_i in Λ. For ease of exposition, we hereby define $\hat{\Lambda} \triangleq \left[\frac{\lambda_1}{q_1}, \cdots, \frac{\lambda_K}{q_K}\right]$ and $Q \triangleq \prod_{i=1}^{K} q_i$.

Theorem C.1.1. *For S_K, a sum of K independent bernoulli-weighted expo-*

[1]Strictly speaking, Λ is a multiset as it may have duplicate elements. For cleaner exposition, however, we call Λ (and other multisets) a set.

nential random variables (as defined above), the CCDF $F^c_{S_K}(\theta) = \Pr\{S_K > \theta\}$ *(for* $\theta \geq 0$*) is given by*

$$F^c_{S_K}(\theta) = Q \sum_{u=1}^{\tau} \sum_{v=1}^{r_u} \left(\sum_{m=0}^{K-1} \left(\alpha_m(\hat{\Lambda}) - \alpha_m(\Lambda) \right) \Upsilon_m(r_u, v) \right) \frac{\mathcal{Q}(v, \delta_u x)}{{\delta_u}^v} \tag{C.1}$$

where

$$\Upsilon_m(r_u, v) = (-1)^{r_u - v} \sum_{\sum_{i=1}^{\tau} n_i = r_u - v} \binom{m}{n_u} {\delta_u}^{m-n_u} \prod_{j \neq u}^{\tau} \binom{r_j + n_j - 1}{n_j} (\delta_j - \delta_u)^{-(r_j + n_j)}. \tag{C.2}$$

The summation in (C.2) is taken over all possible combinations of non-negative integer indices $n_1, \cdots, n_\tau$ *that add up to* $r_u - v$*. Moreover,* $\mathcal{Q}(a, b) = \frac{1}{\Gamma(a)} \int_b^\infty t^{a-1} e^{-t} dt$ *denotes the regularized upper incomplete Gamma function. Furthermore,*

$$\alpha_i(\Lambda) \triangleq (-1)^i \mathcal{C}_\Lambda^{K-i} \tag{C.3}$$

and

$$\mathcal{C}_\Lambda^{K-i} \triangleq \sum^{+} \left[\binom{K}{K-i}_\Lambda \right] \tag{C.4}$$

where $\sum^{+}[\cdot]$ *returns the sum of the elements of the set that it operates on. With a slight abuse of notation,* $\binom{K}{K-i}_\Lambda$ *is defined to be the set of all products of the elements of* Λ *taken* $K - i$ *at a time*[2]*. The summation in (C.4) is taken over the elements of the set* $\binom{K}{K-i}_\Lambda$ *and* $\mathcal{C}_\Lambda^0$ *is defined to be 1. Similarly, the definitions of* $\alpha_i(\hat{\Lambda}) \triangleq (-1)^i \mathcal{C}_{\hat{\Lambda}}^{K-i}$ *and* $\mathcal{C}_{\hat{\Lambda}}^{K-i} \triangleq \sum^{+}[\binom{K}{K-i}_{\hat{\Lambda}}]$*, respectively, follow from (C.3), (C.4) with the set* Λ *now replaced by* $\hat{\Lambda}$*.*

[2]The set $\binom{K}{K-i}_\Lambda$ has cardinality $\binom{K}{K-i}$.

We now give an example to further clarify the notation. For $K = 3$ and $\Lambda = [\lambda_1, \lambda_2, \lambda_3]$, we have $\binom{3}{1}_\Lambda = [\lambda_1, \lambda_2, \lambda_3]$, $\binom{3}{2}_\Lambda = [\lambda_1\lambda_2, \lambda_2\lambda_3, \lambda_3\lambda_1]$ and $\binom{3}{3}_\Lambda = [\lambda_1\lambda_2\lambda_3]$.

C.2 Proof

The following lemma will be used in the proof of Theorem C.1.1.

Lemma C.2.1. *For a set $\Omega = (\omega_1, \cdots, \omega_K)$ consisting of elements which are not all zero, and a variable x, we have the following relation*

$$\prod_{i=1}^{K}(\omega_i - x) = \sum_{i=0}^{K}(-1)^i \mathcal{C}_\Omega^{(K-i)} x^i \tag{C.5}$$

where $\mathcal{C}_\Omega^0 \triangleq 1$.

Proof. The above expression can be verified by expanding both sides in variable x. The proof is omitted for brevity. ■

We now find the characteristic function $\Phi_{\epsilon_i}(jt)$ of $\epsilon_i = z_i G_i$.

$$\Phi_{\epsilon_i}(jt) = \int_{-\infty}^{\infty} e^{jt\gamma} f_{\epsilon_i}(\epsilon)\mathrm{d}\epsilon = q_i + p_i \frac{\lambda_i}{\lambda_i - jt} \tag{C.6}$$

where (C.6) follows by modeling the mixed distribution as $f_{\epsilon_i}(\epsilon) = q_i \mathbb{I}_{(\epsilon=0)} + p_i \lambda_i e^{-\lambda_i \epsilon} \mathbb{I}_{(\epsilon>0)}$, where $\mathbb{I}_{(\cdot)} = 1$ when the condition in the subscript is true and is zero otherwise. We next find the characteristic function of S_K.

$$\Phi_{S_K}(jt) \overset{(a)}{=} \prod_{i=1}^{K} \frac{\lambda_i - q_i jt}{\lambda_i - jt} = \left(\prod_{k=1}^{K} q_k\right) \prod_{i=1}^{K} \frac{\lambda_i q_i^{-1} - jt}{\lambda_i - jt}$$

$$\overset{(b)}{=} \frac{Q\sum_{m=0}^{K}\alpha_m(\hat{\Lambda})y^m}{\sum_{i=0}^{K}\alpha_i(\Lambda)y^i}$$

$$\overset{(c)}{=} Q\left(1+\frac{\sum_{m=0}^{K-1}(\alpha_m(\hat{\Lambda})-\alpha_m(\Lambda))y^m}{\prod_{i=1}^{K}(\lambda_i-y)}\right)$$

$$\overset{(d)}{=} Q\left(1+\sum_{u=1}^{\tau}\sum_{v=1}^{r_u}\frac{\Upsilon_m(r_u,v)}{(\delta_u-y)^v}\right) \tag{C.7}$$

where (a) follows from the property that the characteristic function of a sum of mutually independent random variables equals the product of individual characteristic functions. (b) results by substituting $y = jt$ and applying Lemma C.2.1 to the numerator and the denominator in (a). Adding and subtracting $Q\sum_{i=0}^{K}\alpha_i(\Lambda)y^i$ from the numerator in (b), and using $\alpha_K(\hat{\Lambda}) = \alpha_K(\Lambda)$, we obtain an expression with a proper fraction in (c). Finally, the partial fraction expansion method is used to obtain the result in (d), where

$$\Upsilon_m(r_u,v) = \frac{(-1)^a}{a!}\frac{\partial^a}{\partial y^a}\left[y^m\prod_{i\neq u}^{\tau}(\delta_i-y)^{-r_i}\right]\Bigg|_{y=\delta_u} \tag{C.8}$$

with $a = r_u - v$. Evaluating (C.8) results in (C.2). Applying inverse transform formula on (C.7) gives the probability density function, which upon integration, yields the CCDF of S_K as given in (C.1).

Bibliography

[1] Salam Akoum and Robert W Heath. Interference coordination: Random clustering and adaptive limited feedback. *IEEE Trans. Sig. Proc.*, 61(5-8):1822–1834, Apr. 2013.

[2] J.G. Andrews, F. Baccelli, and R.K. Ganti. A tractable approach to coverage and rate in cellular networks. *IEEE Trans. Commun.*, 59(11):3122–3134, Nov. 2011.

[3] F. Baccelli, B. Blaszczyszyn, and P. Muhlethaler. An Aloha protocol for multihop mobile wireless networks. *IEEE Trans. Inf. Theory*, 52(2):421–436, Feb. 2006.

[4] F. Baccelli and A. Giovanidis. A stochastic geometry framework for analyzing pairwise-cooperative cellular networks. *IEEE Trans. Wireless Commun.*, PP(99):1–1, 2014.

[5] Alessandro Crismani, Udo Schilcher, Stavros Toumpis, Günther Brander, and Christian Bettstetter. Packet travel times in wireless relay chains under spatially and temporally dependent interference. *arXiv preprint arXiv:1311.2698*, 2013.

[6] Harpreet S Dhillon, Radha Krishna Ganti, Francois Baccelli, and Jeffrey G Andrews. Modeling and analysis of K-tier downlink heteroge-

neous cellular networks. *IEEE J. Sel. Areas Commun.*, 30(3):550–560, Apr. 2012.

[7] H.S. Dhillon, Ying Li, P. Nuggehalli, Zhouyue Pi, and J.G. Andrews. Fundamentals of heterogeneous cellular networks with energy harvesting. *IEEE Trans. Wireless Commun.*, 13(5):2782–2797, May 2014.

[8] H. ElSawy, E. Hossain, and M. Haenggi. Stochastic geometry for modeling, analysis, and design of multi-tier and cognitive cellular wireless networks: A survey. *IEEE Commun. Surveys Tuts.*, 15(3):996–1019, Jul. 2013.

[9] D. Gunduz, K. Stamatiou, N. Michelusi, and M. Zorzi. Designing intelligent energy harvesting communication systems. *IEEE Commun. Mag.*, 52(1):210–216, Jan. 2014.

[10] M. Haenggi. On distances in uniformly random networks. *IEEE Trans. Inf. Theory*, 51(10):3584–3586, Oct. 2005.

[11] Martin Haenggi. *Stochastic geometry for wireless networks.* Cambridge University Press, 2012.

[12] Chin Keong Ho and Rui Zhang. Optimal energy allocation for wireless communications with energy harvesting constraints. *IEEE Tran. Sig. Proc.*, 60(9):4808–4818, Sep. 2012.

[13] Kaibin Huang. Spatial throughput of mobile ad hoc networks powered by energy harvesting. *IEEE Trans. Inf. Theory*, 59(11):7597–7612, Nov. 2013.

[14] Ioannis Krikidis. Simultaneous information and energy transfer in large-scale networks with/without relaying. *IEEE Trans. Commun.*, 62(3):900–912, Mar. 2014.

[15] Namyoon Lee, Robert W. Heath, David Morales-Jimenez, and Angel Lozano. Base station cooperation with dynamic clustering in super-dense cloud-RAN. In *IEEE Globecom Workshops*, pages 784–788, Dec. 2013.

[16] Seunghyun Lee, Rui Zhang, and Kaibin Huang. Opportunistic wireless energy harvesting in cognitive radio networks. *IEEE Trans. Wireless Commun.*, 12(9):4788–4799, Sep. 2013.

[17] Gaurav Nigam, Paolo Minero, and Martin Haenggi. Coordinated multipoint in heterogeneous networks: A stochastic geometry approach. In *IEEE Globecom Workshops*, pages 145–150. IEEE, 2013.

[18] O. Ozel, K. Tutuncuoglu, Jing Yang, Sennur Ulukus, and A Yener. Transmission with energy harvesting nodes in fading wireless channels: Optimal policies. *IEEE J. Sel. Areas Commun.*, 29(8):1732–1743, Sep. 2011.

[19] S. Sudevalayam and P. Kulkarni. Energy harvesting sensor nodes: Survey and implications. *IEEE Commun. Surveys Tuts.*, 2011.

[20] R. Tanbourgi, S. Singh, J.G. Andrews, and F.K. Jondral. A tractable model for noncoherent joint-transmission base station cooperation. *IEEE Trans. Wireless Commun.*, 13(9):4959–4973, Sep. 2014.

[21] K. Tutuncuoglu and A Yener. Sum-rate optimal power policies for energy harvesting transmitters in an interference channel. *Journal of Communications and Networks*, 14(2):151–161, Apr. 2012.

[22] S. Ulukus, A. Yener, E. Erkip, O. Simeone, M. Zorzi, P. Grover, and K. Huang. Energy harvesting wireless communications: A review of recent advances. *IEEE J. Sel. Areas Commun.*, 33(3):360–381, Mar. 2015.

[23] C.R. Valenta and G.D. Durgin. Harvesting wireless power: Survey of energy-harvester conversion efficiency in far-field, wireless power transfer systems. *IEEE Microw. Mag.*, 15(4):108–120, Jun. 2014.

[24] R. Vaze. Transmission capacity of wireless ad hoc networks with energy harvesting nodes. In *IEEE Global Conf. on Sig. and Inf. Proc.*, pages 353–358, Dec. 2013.

[25] S. Weber, J.G. Andrews, and N. Jindal. An overview of the transmission capacity of wireless networks. *IEEE Trans. Commun.*, 58(12):3593–3604, Dec. 2010.

[26] A. Zanella, N. Bui, A. Castellani, L. Vangelista, and M. Zorzi. Internet of things for smart cities. *IEEE Internet Things J.*, 1(1):22–32, Feb. 2014.

[27] Rui Zhang and Chin Keong Ho. MIMO broadcasting for simultaneous wireless information and power transfer. *IEEE Trans. Wireless Commun.*, 12(5):1989–2001, May 2013.

Vita

Talha Ahmed Khan is a graduate student at the University of Texas at Austin. He graduated with a Bachelor of Science in Electrical Engineering from University of Engineering and Technology, Lahore in 2010. He started his professional career as an RF Optimization Engineer at Mobilink. Before beginning his graduate studies in 2012, he was affiliated with the Department of Electrical Engineering at Lahore University of Management Sciences, where he worked as a wireless researcher. He was a research intern at Mitsubishi Electric Research Labs, Cambridge during the summer of 2014. He has also interned with the Mobile and Wireless Group at Broadcom, San Diego. His research interests broadly span the areas of wireless communications and networking, with a current focus on green communications.

Permanent address: talhakhan@utexas.edu

This report was typeset with LaTeX[†] by the author.

[†]LaTeX is a document preparation system developed by Leslie Lamport as a special version of Donald Knuth's TeX Program.